Chemical Engineering Journal 480 (2024) 148028

Contents lists available at ScienceDirect

Chemical Engineering Journal

journal homepage: www.elsevier.com/locate/cej

Unveiling the impact of monomer reactivity on the morphology and functionality of thin-film composite membranes

Amirhossein Taghipour [a], Mostafa Dadashi Firouzjaei [a,b], Carolin Ammann [a], Mark Elliott [b], Pooria Karami [a,*], Ahmad Rahimpour [a,*], Mohtada Sadrzadeh [a,*]

[a] Department of Mechanical Engineering, 10-241 Donadeo Innovation Center for Engineering, Advanced Water Research Lab (AWRL), University of Alberta, Edmonton, AB T6G 1H9, Canada

[b] Department of Civil, Construction, and Environmental Engineering, University of Alabama, Tuscaloosa, AL, 35487, USA

ARTICLE INFO

Keywords:
Nanofiltration
Thin film composite (TFC) membranes
Polyesteramide TFC membrane
Polyester membranes
Dye removal
Separation of divalent ions

ABSTRACT

This study delves into the impact of monomer selection and reaction pH on the morphology and performance of thin-film composite (TFC) membranes. The research provides an understanding of how polyamide (PA), polyester amide (PEA), and polyester (PE) membranes can be tailored for specific applications, employing piperazine (PIP) and glucose as monomers in aqueous solution alongside trimesoyl chloride (TMC) as a monomer in an organic solution. PEA-based membranes containing glucose demonstrated several notable improvements, including a reduced contact angle of 60 degrees, a smoother surface, and a more negative zeta potential. These enhancements underscore their increased hydrophilicity, decreased susceptibility to fouling, and heightened surface charge. Controlling pH during fabrication significantly changed the membrane surface charge, hydrophilicity, water flux, and rejection rate. At pH 11, the PA membrane excelled in rejection performance (99.5% Na2SO4, 32% NaCl, and 97.8% methyl orange) with a trade-off in lower water flux (56 LMH). Conversely, the PE membrane achieved the highest water flux (173 LMH) but lower rejection (58% Na2SO4, 10% NaCl, and 97% methyl orange). The PEA membrane offered notable water flux (82.5 LMH) and high rejection for methyl orange (99.3%) and Na2SO4 (99.2%). Increasing the pH reduced permeation rates but enhanced rejection, especially for NaCl. The PE and PEA membranes exhibited remarkable antifouling properties, boasting a flux recovery ratio compared to the PA membrane. This study highlights the pivotal role of monomer selection and pH control in TFC membrane performance, offering prospects for innovative design and optimization in water treatment membrane technology.

1. Introduction

With the world's increasing population and unequal access to safe water, seawater desalination and wastewater reclamation have become indispensable [1,2]. The versatility of membrane technology across these diverse fields underscores its significance in addressing global water challenges, improving resource management, and contributing to environmental sustainability [3]. Its high separation performance and compact design make it economically viable [4], especially for remote and rural communities. Nanofiltration (NF), a type of membrane technology, has emerged as a promising solution for water softening, selective ion removal, and dye, chemical, and pharmaceutical separation. NF relies on semi-permeable membranes, primarily thin film composite (TFC) membranes, as its central component for efficiently eliminating a wide range of water pollutants [5,6]. TFC membranes are typically synthesized by the interfacial polymerization reaction, which takes place at the interface of an organic solution containing acyl chlorides, e.g., trimesoyl chloride (TMC), and an aqueous solution containing amine monomers, e.g., piperazine (PIP) and m-phenylenediamine (MPD) [7–9]. While existing polyamide TFC membranes have superior permselectivity, there has been a significant increase in research over the past decade to discover environmentally friendly monomers. These monomers are sought to either maintain or surpass the performance and antifouling characteristics of TFC membranes created with conventional amine monomers [10,11].

The widespread use of monomers derived from crude oil, such as MPD or PIP, in membrane manufacturing presents environmental challenges due to their non-biodegradability and the potential for

* Corresponding authors.
E-mail addresses: pkarami@ualberta.ca (P. Karami), arahimpo@ualberta.ca (A. Rahimpour), sadrzade@ualberta.ca (M. Sadrzadeh).

https://doi.org/10.1016/j.cej.2023.148028
Received 11 September 2023; Received in revised form 2 November 2023; Accepted 9 December 2023
Available online 14 December 2023
1385-8947/© 2023 Elsevier B.V. All rights reserved.

contaminating ecosystems. This poses risks to aquatic life [12] and potential ingress into food chains [13,14]. In response, innovative chemistries have recently been explored as replacements for the conventional polyamide structure of TFC membranes to improve permselectivity, chlorine resistance, and antifouling properties [15–17]. Bio-monomers like cyclodextrin, tannic acid, catechol, and dopamine have demonstrated promise in fabricating TFC membranes with improved separation performance [18–20]. However, these bio-monomers are relatively rare and require complex extraction procedures, which can raise the overall cost of membrane fabrication. As a result, there has been considerable interest in utilizing eco-friendly and renewable sugar-based materials for the synthesis of NF membranes. Monomers such as maltose, raffinose, and glucose have garnered significant attention due to their water solubility, non-toxic nature, and abundance in plant tissues [10]. Crosslinking these bio-monomers with acid chloride monomers makes it possible to create polyester chains with distinctive properties, including high hydrophilicity and a negative surface charge [10]. However, due to the low reactivity of acyl chloride and hydroxyl groups, this process may form loosely structured polyester (PE) NF membranes, resulting in suboptimal salt rejection. To address this issue, it is essential to delve into the underlying mechanisms and explore innovative approaches that can enhance the reactivity of these groups. One promising avenue involves the manipulation of reaction conditions, such as increasing the reaction temperature [21] or adjusting the alkalinity of the reaction environment. These adjustments can facilitate the consumption of the produced acid molecules in the interfacial polymerization reaction and accelerate the shift of the reaction toward the formation of a more crosslinked PA layer.

Several strategies have been employed to enhance the separation performance of polyester NF membranes. Shen et al., for example, used a novel fabrication method known as thermal-facilitated interfacial polymerization to create high-performance NF membranes with glucose [21]. Elevating the temperature during interfacial polymerization improved the diffusion of glucose monomer to the interface and accelerated reaction rates, resulting in PE membranes with high crosslinking, Na_2SO_4 rejection, and water permeability. Concurrently, efforts have been directed toward developing polyesteramide membranes with enhanced crosslinking and antifouling properties by incorporating multiple monomers into the aqueous phase [2218]. It's worth noting that carbohydrate-based monomers with phenolic branches may exhibit lower water solubility, possibly necessitating alkaline conditions to achieve sufficient solubility [23]. Under such conditions, catalysts like sodium hydroxide are essential to facilitate the polycondensation reaction, improving the final structure and properties of TFC membranes [24]. Therefore, by judiciously selecting the monomers and carefully controlling the reaction conditions, it is possible to develop NF TFC membranes with superior permselectivity and antifouling performance.

The novelty of this work lies in its comprehensive exploration of the fabrication process for polyesteramide TFC membranes. We first investigated the effect of the monomer ratio (glucose/PIP) on the performance of polyesteramide TFC membranes in terms of water permeability, salt and dye rejection, and antifouling properties. Upon identifying the optimal monomer ratio, we broaden our investigation to examine the role of alkalinity in membrane fabrication. Our findings unveiled the pivotal roles played by both monomer ratio and pH level in the performance of polyesteramide TFC membranes. Consequently, this study contributes novel insights into the membrane fabrication process and lays the foundation for developing more efficient membrane technologies. Such advancements align seamlessly with global objectives for sustainable and superior water treatment solutions.

2. Materials and methods

2.1. Materials

The polyethersulfone membrane support (PES, MWCO: 100 kDa) was procured from Sterlitech Corporation. Sodium chloride (NaCl, $\geq$ 99%), sodium sulfate (Na_2SO_4, $\geq$ 99%), and sodium hydroxide (NaOH, $\geq$ 97%) were purchased from Sigma-Aldrich. Glucose (GL, MW: 182.14 g/mol), PIP (MW: 86.14 g/mol), trimesoyl chloride (TMC, 98 %), and n-heptane were obtained from Fisher Scientific. Methyl orange (MO), sodium alginate (SA), and bovine serum albumin (BSA) were supplied by Sigma-Aldrich and used as a negatively charged dye and organic foulants in the filtration experiments. Deionized water (DI) was used to prepare aqueous solutions. All solvents and chemicals were of reagent grade and used as received.

2.2. Fabrication of the TFC membranes

Polyester (PE), polyamide (PA), and polyesteramide (PEA) TFC membranes were synthesized by an interfacial polymerization involving glucose/TMC, PIP/TMC, and PIP-glucose/TMC, respectively. Fig. 1 shows the schematic illustration of the fabrication procedure for these TFC membranes. First, the PES support was saturated with an aqueous solution containing different concentrations of PIP and glucose dissolved in an alkaline NaOH solution (with a fixed pH of 12). A polymethacrylic acid roller removed The excess aqueous solution from the support surface. Subsequently, an organic solution of 0.2 wt% TMC in n-heptane was applied to the support to initiate polymerization, and the reaction was allowed to proceed for 5 min. The resulting TFC membrane was cured in an oven at 75 °C for 10 min to complete the reaction and was then rinsed with DI water. In the second phase, a series of membranes were produced by adjusting the pH levels for the optimal membranes (selected based on separation performance) using the same procedure. Table 1 details the membrane samples' labeling, composition, and synthesis pH.

2.3. Characterization of membranes

Morphological characteristics of synthesized membranes were explored with microscopic analysis, including field emission-scanning electron microscopy (FE-SEM, Zeiss Sigma 300 VP) and transmission electron microscopy (TEM, Philips/FEI Morgagni 268). The surface topography of the fabricated TFC membranes was evaluated using atomic force microscopy (AFM, Bruker Dimension Icon, USA) analysis over a surface area of 100 μm^2. All AFM measurements were carried out in tapping mode at a scan rate of 1.0 Hz in ambient temperature and humidity conditions. The AFM data were analyzed using nanoscope analysis software. Attenuated total reflectance-Fourier transform infrared (ATR-FTIR) was utilized to analyze the chemical composition of the produced membranes. The infrared spectra were recorded at ambient temperature using Agilent Technologies, Cary 600 series. All the samples were subjected to 30 scans covering the wavelength range of 400–4000 cm^{-1} with a resolution of 4 cm^{-1}.

A Surpass™ 3 Electrokinetic analyzer (Anton Paar, Graz, Austria) was utilized to measure the zeta potential of the membranes over the pH range of 4–9 using a 1 mM KCl solution. To adjust the pH of the KCl solution, sodium hydroxide and hydrochloric acid were injected into the solution over the experiments. The surface charge of the membranes was measured at least three times to evaluate the repeatability, and the obtained values were finally averaged and reported. To evaluate the surface wettability of the membranes, a contact angle analysis (Kruss DSA 100 Gmbh Germany) was performed using the sessile drop method. A 2 μL droplet of DI water was placed on the membrane surface. At least ten droplets were placed on the surface of each sample, and the resulting average contact angles were measured and recorded.

2.4. Membrane filtration tests

All filtration experiments were performed using a cross-flow filtration setup with a feed flow rate of 2 L/m and a transmembrane pressure of 70 psi. The feedwater temperature was maintained at 25 $\pm$ 3 °C using

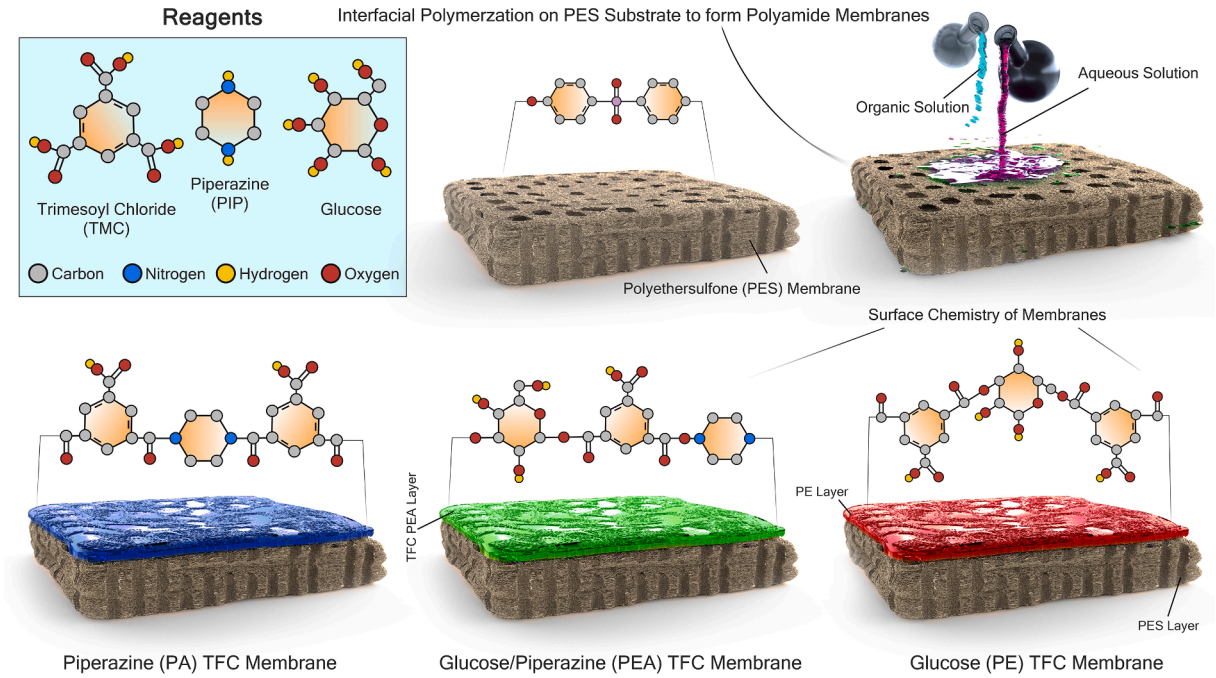

Fig. 1. The schematic illustration of the membrane's structures and surface chemistry. Interfacial polymerization of glucose/TMC, PIP/TMC, and PIP-glucose/TMC produced polyester (PE), polyamide (PA), and polyesteramide (PEA) TFC membranes. Aqueous solution impregnated the PES support first. An aqueous solution of PIP and glucose in NaOH (pH 12) contained different concentrations. An acrylic roller removed the aqueous solution from the membrane. The support was poured with 0.2 w.t% TMC in n-heptane to start polymerization. The TFC membrane was treated at 75 °C for 10 min to finish the reaction and washed with DI water. The second phase involved varying pH levels to create a series of membranes with the best separation performance.

Table 1
Membranes' composition and labeling information. The last part of the label shows the pH condition of IP. For PEA membranes, the percentage in the middle shows the glucose concentration.

Membrane	Glucose (wt.%)	PIP (wt.%)	pH	Sample Label
Polyester	10	0	11	PE-11
	10	0	12	PE-12
	10	0	13	PE-13
Polyesteramide	4	0.1	12	PEA-4 %-12
	7	0.1	12	PEA-7 %-12
	10	0.1	11	PEA-10 %-11
	10	0.1	12	PEA-10 %-12
	10	0.1	13	PEA-10 %-13
Polyamide	0	0.1	11	PA-11
	0	0.1	12	PA-12
	0	0.1	13	PA-13

a Fisher Scientific Isotemp 3013 circulating chiller water bath. The Sterlitech CF016 cross-flow filtration cell was used with an active membrane surface area of 20.6 cm^2, slot depth of 0.23 cm, and slot width of 0.39 cm. Before adding solutes/foulant, a pure water filtration experiment was conducted for 2 h at 70 psi until there was no change in water flux readings. The permeate water was collected on a digital balance, and the permeate water flux (*Jw*) was calculated as follows:

$$J_w = \frac{\Delta m}{A\,\Delta t} \tag{1}$$

Where Δm is the mass variation of the collected permeate, A is the active surface area, and Δt is the time interval. After membrane compaction, solute/foulant solutions such as salts, dye, and foulant were replaced with pure water in the feed tank. The rejection percentage (R) was calculated using the following equation:

$$R = \left[\frac{C_f - C_p}{C_f}\right] \times 100 \tag{2}$$

where C_p and C_f are the concentrations of solutes in the permeate and feedwater.

2.5. Antifouling experiments of membranes

To assess the antifouling capabilities of the membranes, fouling experiments were conducted using various foulants, including BSA (100 ppm), SA (150 ppm) with $CaCl_2$, and MO (150 ppm). The pure water flux was initially measured for 30 min (J_{wi}). Subsequently, the foulant solution was introduced to the feed solution, and the flux was continuously monitored for 5 h (J_s). Finally, thorough cleaning was conducted with a high flow rate of pure water to remove any residual foulant. After cleaning, the pure water flux was measured again (J_{wf}) for 30 min. The flux recovery ratio (FRR) and flux decline rate were calculated as FRR = J_{wf}/J_{wi} and FD = J_{wi}-J_s/J_{wi}, respectively [25,26]. To further evaluate the antifouling characteristics of the membranes, the fouling tests were repeated in a second cycle, following the same protocol. In both cycles, the membranes were subjected to the same initial pure water flux (J_{wi}) to maintain consistent fouling conditions.

3. Results and discussion

3.1. Membrane surface morphology characterization

The structure of the final thin selective polymer layer can be tuned by monomer's reactivity behavior [27]. The high reactivity of PIP and TMC leads to an immediate and intense reaction at the interface of the two solutions, where polymerization occurs. Because the polymer chains do not have enough time to arrange themselves into a smooth and homogeneous structure, the surface becomes relatively rough and non-uniform [28]. Given PIP's impact in promoting roughness and heterogeneity in the synthesized polymer film, the PIP concentration was deliberately reduced to 0.1 wt% to ensure the uniformity and structural integrity of the membrane.

Cross-sectional TEM images of the PE-12, PA-12, and PEA-10 %-12

membranes, prepared at a pH of 12, confirm the formation of thin selective layers on the support membranes, as shown in Fig. 2**a**. Notably, PE-12, PEA-10 %-12, and PA-12 membranes showed an average selective layer thickness of 50 nm. One of the key factors in fabricating high-performance TFC membranes is to achieve the critical balance between monomer reactivity and its concentration during polymerization. The smart adjustment of these parameters will produce a thin and uniform polymeric layer, thereby enhancing the performance of the resulting membranes. Further analysis of the surface morphology was conducted via AFM and SEM analyses.

Shifting from polyamide to polyester structure (PA to PE), the average and mean square roughness values were reduced from 46 nm and 57.2 nm to 29.9 nm and 43.4 nm, respectively (Fig. 2). The top SEM images showed a completely different morphology of the polyester membrane (PE-12) from that of the polyamide (PA-12). TFC membranes with polyester linkages showed spherical-like structures, whereas polyamide displayed nanoscale fiber-like shapes (Fig. 2**b**). The AFM and FE-SEM images of the PA-12 membrane revealed a distinct fiber-like structure (resembling nanoscale stripes [29]). In contrast, the polyesteramide TFC membrane (PEA-10 %-12) revealed a hybrid structure of polyester and polyamide membranes. This included spherical chambers akin to those found in PE-12, as well as a fiber-like structure reminiscent of PA-12. Importantly, both the PA and PEA membranes exhibited a consistent and uniform morphology devoid of irregularities. This

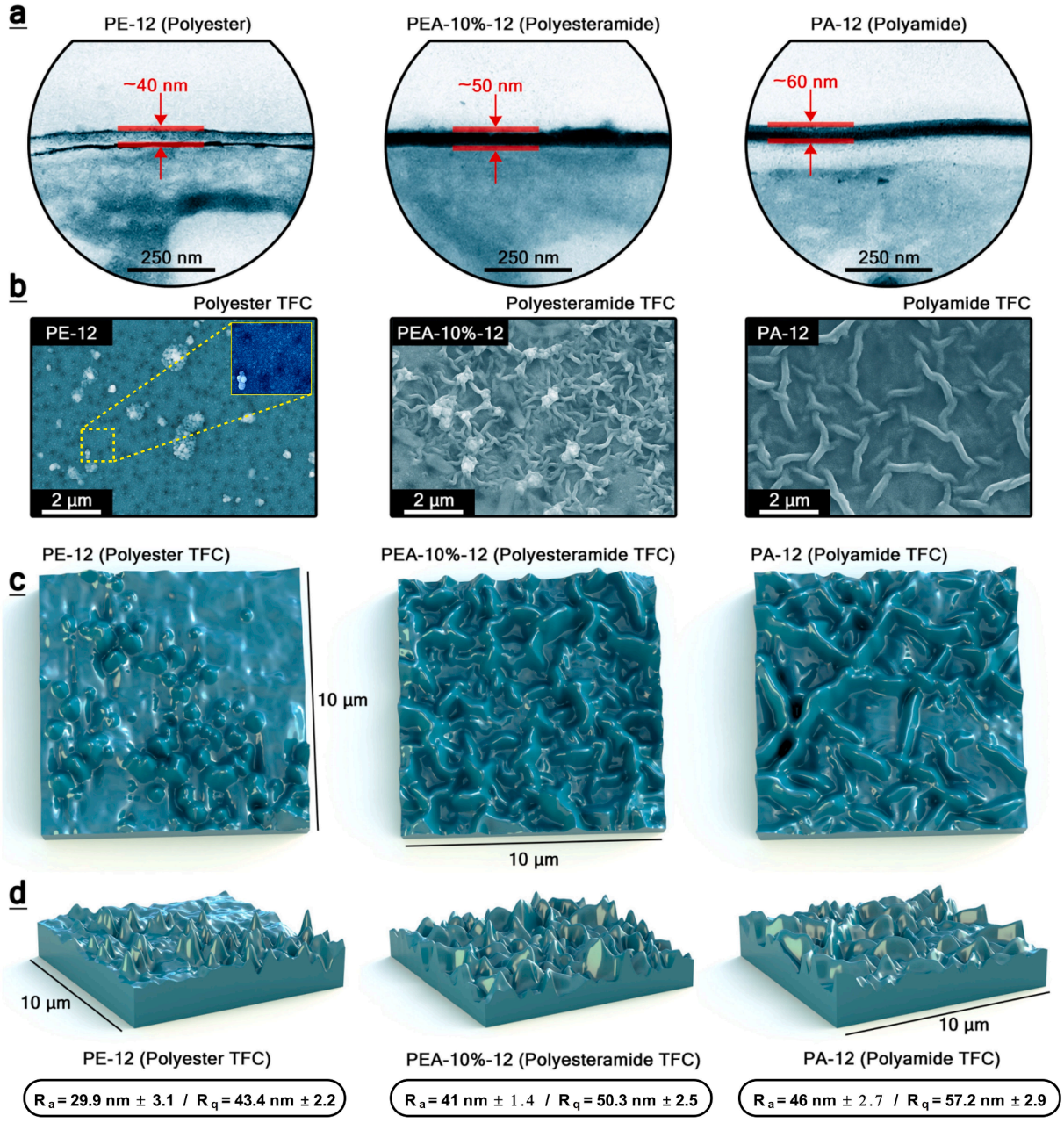

Fig. 2. Images of (a) the cross-sectional TEM and (b) the top surface SEM of the synthesized thin-film composite (TFC) membranes. (c) top view and (d) side view AFM renders of the membranes. The images demonstrate that all fabricated membranes have a homogeneous formation of selective layers atop the supporting structure. Despite the inherent challenges posed by the piperazine (PIP) and trimesoyl chloride (TMC) monomers' rapid reactivity and diffusivity, we achieved relatively thin and uniformly structured selective layers. Notably, the average thickness of the polyester and polyamide membranes is 40 nm and 60 nm, respectively, while the polyesteramide composite has an optimum thickness of 50 nm. Such thickness variations reveal the delicate balance between reactant concentration and reactivity. The visual evidence validates the method's effectiveness in generating thin, uniform selective layers, a critical determinant of TFC membrane performance.

observed uniformity is likely due to the compatibility between the TFC layer and the PES support material. The hybrid PEA membrane demonstrated intermediate structural features and exhibited roughness values falling within the range of the corresponding values of PA and PE membranes. Specifically, the PEA membrane's average and mean square roughness were measured at 41 nm and 50 nm, respectively.

The disparities in surface morphology and roughness differences between PE and PA TFC membranes can be attributed to their respective monomers' distinct transport and reaction characteristics. In the case of the PE-12 membrane, glucose monomers undergo esterification with the acyl chloride groups of TMC, forming ester bonds (−COO–) that connect multiple glucose units covalently [21]. This creates a more uniform polymer network, contributing to smoother surface morphology. Additionally, the numerous hydroxyl groups in glucose have the potential to form hydrogen bonds with other monomers or functional groups, further influencing the organization and packing of polymer chains and reducing surface roughness. Finally, the larger size of glucose molecules (MW: 182.14 g/mol) compared to PIP (MW: 86.14 g/mol) decreased their diffusion to the reaction zone in the organic phase, leading to a thinner and smoother selective layer [30,31]. In contrast, for the PA-12 membrane, PIP monomers react with the acyl chloride groups of TMC via amide bond formation, polymerizing into polyamide chains. Chain extension reactions in PIP monomers form long, interconnected polymer chains, contributing to fiber-like surface morphology. In summary, the specific interplay between monomer transport properties, reactivity, reaction kinetics, and crosslinking extent in both PE and PA membranes played a pivotal role in shaping their unique surface characteristics. Furthermore, the introduction of glucose in the aqueous phase during the fabrication of the PEA membrane reduced its roughness, indicating the influence of glucose on regulating the polymerization process.

3.2. Membrane surface chemical and physicochemical characterization

The chemical composition of membranes was characterized by FTIR and XPS spectroscopy (Fig. 3). The appearance of the characteristic amide peak at 1610 cm^{-1} (aromatic amide ring stretching) and the ester peak at 1728 cm^{-1} (C═O stretching of ester bonds) confirms the formation of amide and ester linkages over the PES substrate [21,22,32–34]. Comparing the spectra of PEA membranes shows that an increase in glucose concentration from 4 to 10 wt% led to a noticeable decrease in the intensity of the amide peaks, coupled with an increase in the intensity of the ester peaks. This increased intensity of ester linkages suggests that glucose played a more substantial role in forming the selective layer at higher glucose concentrations. Furthermore, the peak

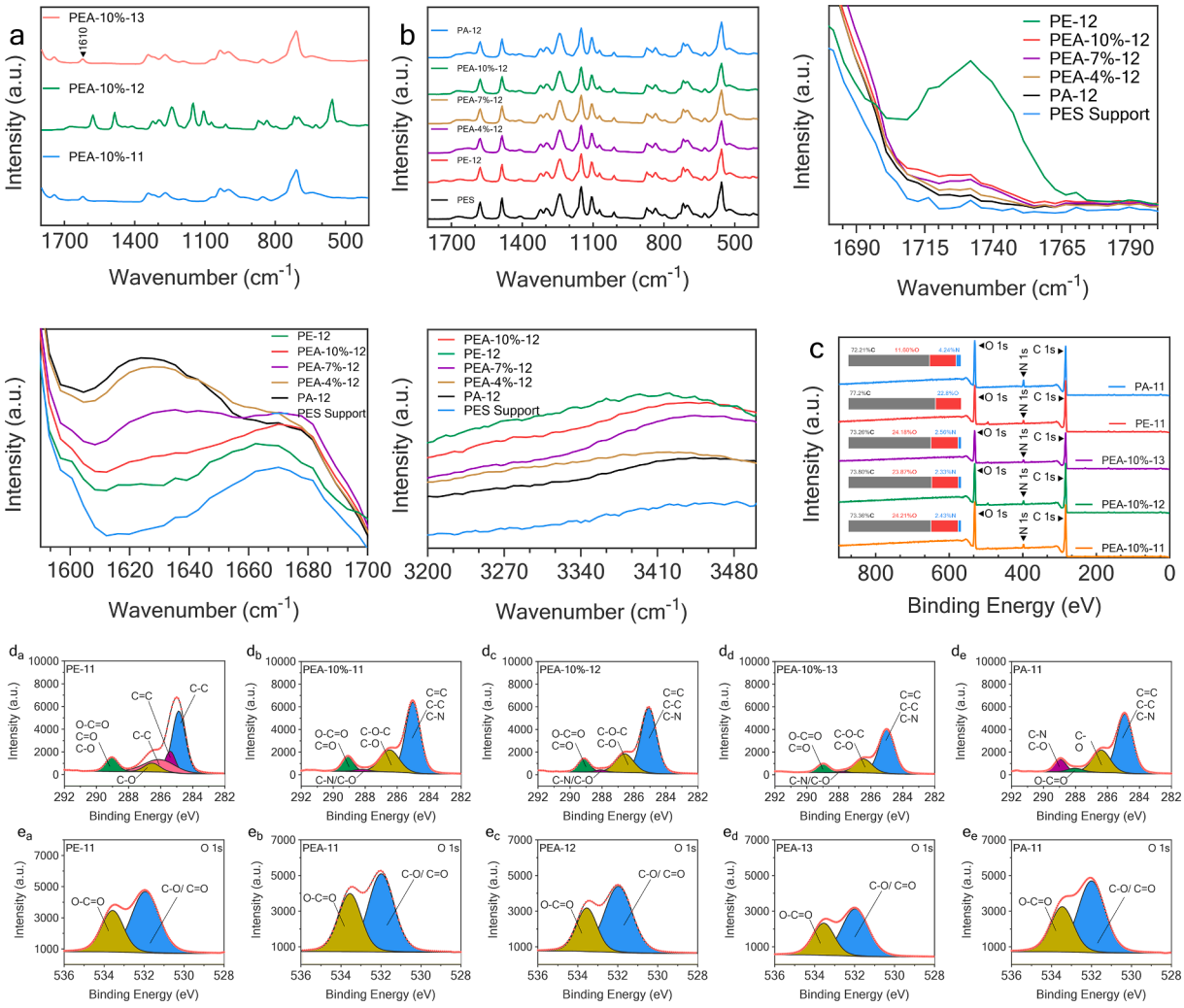

Fig. 3. (a) FTIR spectra of the fabricated membranes. (b) XPS survey spectra of the membranes with their elemental composition. High-resolution (c) C1s and (d) O1s XPS spectra of the membranes. According to FTIR and XPS spectroscopy analyses, the incorporation of glucose monomers increases the intensity of ester linkages and hydroxyl groups, indicating their contribution to the selective layer. The amide bond content and hydroxyl groups in membranes synthesized at higher pH levels decrease, potentially impacting hydrophilicity and crosslinking. Aliphatic and aromatic carbon structure concentrations vary across the membranes, affecting rigidity, mechanical resistance, and water flux. The presence of PIP causes an increase in aromatic character, which may improve membrane resistance.

corresponding to the hydroxyl groups at 3450 cm^{-1} also showed an apparent increase with increasing the glucose concentration, indicating the presence of more free hydroxyl groups in the selective layer. The FTIR spectra of the polyesteramide membranes at different pH levels were also compared. The results revealed a clear drop in the amide peak intensity (at 1610 cm^{-1}) as the alkalinity of the aqueous phase increased. Additionally, the peak corresponding to the free hydroxyl group at 3450 cm^{-1} decreased, indicating that more free hydroxyl groups of the glucose monomer contributed to the reaction at elevated pH levels.

Fig. 3 shows the survey and high-resolution XPS spectra of the synthesized membranes. Table 2 provides information on the abundance and intensity distribution of different functional groups of the C1s for these membranes. Regarding the high-resolution XPS data of carbon, the PE-12 membrane exhibits the highest concentration of aliphatic carbon structures (C–C) at 47.45 %, with successive membranes (from PEA-4 %-12 to PA-12) showing a decrease in this component. The prevalence of aliphatic characteristics in the PE-12 membrane implies that it may possess lower rigidity than the subsequent membranes. The transition from PE-12 to PA-12 membranes reveals a significant increase in the proportion of aromatic carbon structures (C═C or C-C) within the TFC layer. Remarkably, the PEA-10 %-12 and PEA-10 %-13 membranes exhibit the highest aromatic carbon concentration, measuring at 66.57 % and 65.55 %, respectively. This higher aromatic content in these membranes can affect their permeability and selectivity. Due to their rigid and planar nature, aromatic carbon structures can impact the overall packing of molecules within the membrane, potentially influencing the permeability of different solutes through the membrane [35].

The carbonyl (C═O) group content remains relatively stable across all membranes, with only minor variations observed. The concentration of carboxylic (O–C═O) groups in glucose-containing membranes remains mostly constant, except for a notable decrease in PA membranes. This decrease is associated with an increase in the negative surface charge of membranes, contributing to their improved rejection. Comparing PE-11 and PEA-10 %-11 (both with 10 % glucose) to PA-11 (0 % glucose) reveals that the presence of glucose leads to a higher percentage of hydroxyl groups (C–O bond in C–OH structure) and ether bonds (C–O–C). This observation suggests that the incorporation of glucose increases the hydrophilicity of the membrane, which has the potential to improve water flux performance. Therefore, it is anticipated that the PEA membranes may exhibit enhanced selectivity and fouling resistance.

Comparing the membranes with varying pH values, namely PEA-10 %-11 (pH = 11), PEA-10 %-12 (pH = 12), and PEA-10 %-13 (pH = 13), it can be observed that the percentage of hydroxyl groups (C–O bond in C–OH structure) and ether bonds (C–O–C) slightly decreases with increasing pH. Additionally, the content of amide bonds (C–N/C–O), which form during the reaction of TMC with glucose or PIP, decreases with an increase in pH. This reduction is evident from the decrease in content from 2.02 % (PEA-10 %-11) to 1.61 % (PEA-10 %-12) and 1.32 % (PEA-10 %-13). These observations suggest that pH can influence the hydrophilicity and crosslinking of the membrane. Higher pH values result in enhanced salt rejection and reduced water flux, possibly due to the formation of a denser selective layer network. Higher pH values can lead to increased deprotonation of the amine groups, resulting in a higher concentration of reactive amine species [36]. This increased reactivity can promote the formation of a more extensive selective polymer network with a higher degree of crosslinking. Moreover, increased pH can accelerate the reaction kinetics between the amine and acyl chloride groups, leading to faster network formation [24]. This accelerated reaction may result in a more interconnected and denser polyamide structure. The pH can also influence the organization of the polyamide chains within the network. Higher pH values can promote a more ordered arrangement of the chains, leading to a denser and more compact structure.

Table 2
The abundance and intensity distribution of various C1s peaks of the membranes.

Membrane/ Carbon 1 s Deconvolution Information	Binding Energy (eV)	Relative Concentration (%)
PA-11		
C═C (Aromatic ring in TMC), C-C (Aromatic ring in TMC), C-N (Piperazine)	284.92	61.05
C-O (Carboxylic group in TMC)	286.38	25.73
O-C═O (Carboxylic group in TMC), C═O (Carbonyl group in TMC)	288.03	3.86
C-N/C-O (Amide bond from the reaction of TMC with water/Piperazine)	288.95	9.36
PE-11		
C-C (Aliphatic carbon structures in glucose or TMC)	284.86	47.45
C-O (Hydroxyl group in glucose)	286.53	8.09
O-C═O (Carboxylic group in TMC), C═O (Carbonyl group in TMC), C-O (Amide bond from the reaction of TMC with water/glucose or ether bond from glucose)	289.04	9.65
C═C (Aromatic ring in TMC)	285.39	12.53
C-C (Carbon backbone in glucose)	286.08	22.28
PEA-10 %-11		
C═C (Aromatic ring in TMC), C-C (Aromatic ring in TMC), C-N (Piperazine)	285.01	62.71
C-O-C (Ether bond in glucose), C-O (Hydroxyl group in glucose)	286.46	25.38
O-C═O (Carboxylic group in Trimesoyl Chloride), C═O (Carbonyl group in TMC)	289.09	9.9
C-N/C-O (Amide, and ester bonds respectively from the reaction of TMC with piperazine and glucose or ether bond from glucose)	288.19	2.02
PEA-10 %-12		
C═C (Aromatic ring in Trimesoyl Chloride), C-C (Aromatic ring in Trimesoyl Chloride), C-N (Piperazine)	285.07	66.57
C-O-C (Ether bond in glucose), C-O (Hydroxyl group in glucose)	286.58	21.9
O-C═O (Carboxylic group in TMC), C═O (Carbonyl group in TMC)	289.12	9.92
C-N/C-O (Amide, and ester bonds respectively from the reaction of TMC with piperazine and glucose or ether bond from glucose)	288.08	1.61
C═C (Aromatic ring in Trimesoyl Chloride), C-C (Aromatic ring in Trimesoyl Chloride), C-N (Piperazine)	285.07	66.57
C-O-C (Ether bond in glucose), C-O (Hydroxyl group in glucose)	286.58	21.9
PEA-10 %-13		
C═C (Aromatic ring in Trimesoyl Chloride), C-C (Aromatic ring in TMC), C-N (Piperazine)	285	65.54
C-O-C (Ether bond in glucose), C-O (Hydroxyl group in glucose)	286.46	23.08
O-C═O (Carboxylic group in TMC), C═O (Carbonyl group in TMC)	288.98	10.06
C-N/C-O (Amide, and ester bonds respectively from the reaction of TMC with piperazine and glucose or ether bond from glucose)	287.74	1.32
C═C (Aromatic ring in TMC), C-C (Aromatic ring in TMC), C-N (Piperazine)	285	65.54

3.3. Wettability and surface charge of the fabricated TFC membranes

Fig. 4 shows that the membrane's surface becomes more negative as the concentration of glucose increases. This increase in negative charge is due to increased carboxyl functional groups and their deprotonation in water [21]. The higher negative surface charge can enhance the rejection of negatively charged contaminants [37]. Furthermore, a high negative charge can reduce membrane fouling by repelling foulants, often possessing negative charges in water due to electrostatic repulsion

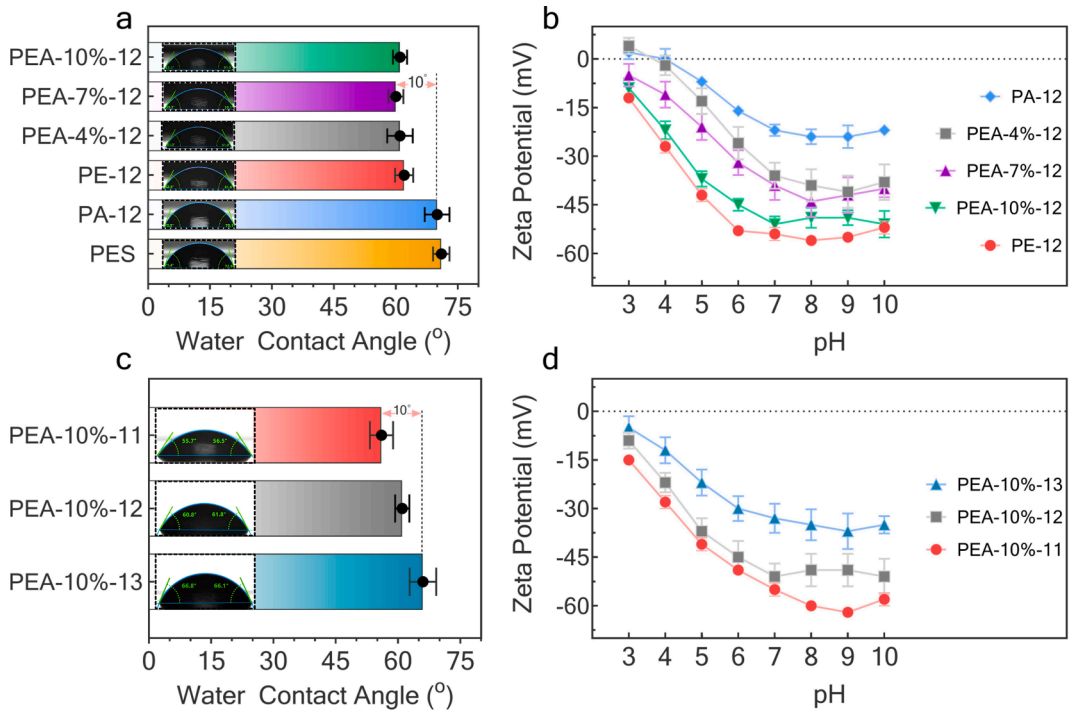

Fig. 4. Contact angle and zeta potential results of the fabricated membranes with (a,b) different monomer ratios and (c,d) different pH levels. As glucose concentration increases, the membrane surface becomes more negatively charged and hydrophilic due to increased hydroxyl functional groups and ester linkages. This shift can enhance the rejection of certain contaminants and reduce membrane fouling. However, as the pH increases, the formation of amide linkages increases, altering the surface properties by decreasing the membrane's negative charge and reducing its hydrophilicity. These changes emphasize the significance of controlling and optimizing pH during the membrane fabrication process to achieve the desired performance.

[38]. The contact angle is a measure of a membrane's wettability. A lower contact angle indicates greater hydrophilicity, which improves water permeability and reduces fouling [39]. The PEA membrane has a lower contact angle (around 60°) than the PA-12 membrane (71°), indicating improved hydrophilicity due to the greater amount of hydroxyl groups and ester linkages. The similarity in contact angle values among PE-12, PEA-10 %, PEA-7 %, and PEA-4 % membranes can be partially explained by Wenzel's equation. Wenzel's equation describes how surface roughness can amplify the wettability influenced by the surface chemistry. In simpler terms, when a surface is chemically hydrophilic, the addition of surface roughness amplifies its hydrophilic nature. This principle, as elucidated by Wenzel, can be explained as follows [40,41]:

$$cos\theta_m = rcos\theta_y \quad (3)$$

In this equation, θ_m represents the measured contact angle, θ_y corresponds to Young's contact angle, and r signifies the roughness ratio. The roughness ratio is the ratio between the actual solid surface area and the projected surface area, with $r = 1$ denotes a smooth surface and $r > 1$ indicates a rough surface. In this study, the transition from PA to PE and PEA membranes resulted in a noticeable reduction in surface roughness. This reduction would typically lead to an increase in hydrophobicity, as indicated by higher contact angles. However, this effect is counterbalanced by the intrinsic hydrophilic nature of the fabricated polyester and polyesteramide TFC membranes.

Fig. 4**c and d** show the impact of pH on the wettability and surface charge of the fabricated TFC membranes. During the interfacial polymerization reaction, as the pH of the aqueous solution rises, more amide linkages form [36], increasing crosslinking density and altering the surface properties. This increase in amide linkages (or decrease in free $–NH_2$ groups) and a decrease in carboxyl groups make the membrane less negatively charged. Furthermore, an increase in pH increases contact angle, indicating a reduction in hydrophilicity. This trend is consistent with the hypothesis that increasing the number of monomer linkages reduces the number of free–COOH groups, resulting in lower hydrophilicity. This pH-dependent behavior highlights the importance of pH control in the membrane fabrication process and emphasizes the need to optimize the pH to achieve desirable membrane characteristics.

3.4. *Transport performance of the fabricated membranes*

The transport performance of membranes is presented in Fig. 5. PE membranes typically provide higher flux values than PA and PEA membranes. PE-11 has the highest water flux of 173 LMH among the membranes, while PE-13 has the lowest water flux of 33.6 LMH. Regarding rejection percentages, PA membranes tend to achieve higher rejection rates than PE and PEA membranes. In particular, PA-11 exhibits the highest rejection percentages for Na_2SO_4 (99.5 %), NaCl (32 %), and methyl orange (97.8 %). Nevertheless, the PE and PEA membranes also achieve significant rejection rates, with PE-12 and PEA-10 %-13 surpassing 95 % and 65 % rejection rates for Na_2SO_4 and NaCl, respectively.

When comparing the three types of membranes, the PEA membranes fall in between the PA and PE membranes regarding both water flux and rejection percentages. PEA-10 %-12 exhibits a moderate water flux of 58 LMH and a high Na_2SO_4 rejection percentage of 99 %. However, there are variations within each membrane type depending on specific synthesis conditions such as pH and concentration. When we examine membranes synthesized at different pH levels, several trends emerge: (i) The water flux in the PE membranes decreases significantly as the pH rises from 11 to 13. PE-11 has the highest water flux at 173 LMH, while PE-13 has the lowest at 33.6 LMH. (ii) Similar trends are observed for PA and PEA membranes at different pH levels. For instance, when compared to PEA-10 %-13 (48.9 LMH), PEA-10 %-11 exhibits a higher water flux at 82.5 LMH. Overall, it is evident that pH variation during membrane synthesis has a substantial impact on membrane water flux, particularly for the PE and PEA membranes. Higher pH values tend to result in lower

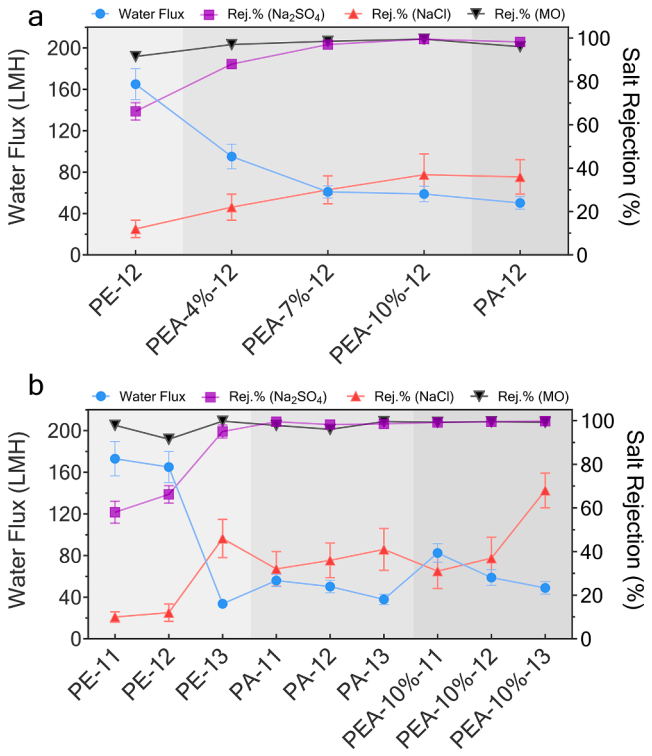

Fig. 5. Filtration results of the fabricated TFC membranes at (a) different monomer ratios and (b) pH levels. There are distinct trends in the performance of PA, PE, and PEA membranes. PE membranes have greater water flux, whereas PA membrane has a greater rejection percentage. In terms of performance, PEA membranes fall somewhere in the middle. Water flux is significantly affected by pH variation during membrane synthesis, with higher pH resulting in lower flux. Water flux and salt rejection are influenced by the presence of glucose monomers, with higher glucose concentrations resulting in higher rejection. Alkalinity increases salt rejection even more. The interaction of glucose and TMC influences dye rejection.

water flux and higher rejection rates.

To better understand the observed filtration results, it is essential to consider the principles of size exclusion and Donnan exclusion as the fundamental mechanisms behind NF separation. In the size exclusion mechanism, the polymeric layer's pores hinder the passage of larger solutes, such as SO_4^{2-}. Then, to preserve electroneutrality on the permeate side, the passage of Na^+ is also hampered. The Donnan exclusion can be attributed to the negatively charged surface of the TFC layer, which facilitates electrostatic repulsion, thereby repelling the negatively charged solutes. Regarding the influence of pH, it was evident that an increase in alkalinity led to a reduction in water flux across all samples, simultaneously resulting in an enhancement of salt and dye rejection. This aligns with previous literature findings, which demonstrated that elevated alkalinity accelerates crosslinking during polymerization [36]. As a result, the synthesized polymeric structure displayed a higher crosslinking density at elevated pH levels, contributing to exceptional rejection properties based on size exclusion. The control of pH plays a pivotal role in our experiments. Elevated pH serves as a catalyst by consuming the byproduct acid, thereby driving the polycondensation reaction further to the right side, promoting the formation of more crosslinked structures. In practical terms, elevating the reaction's pH within the fixed reaction time of 5 min results in the contribution of more monomers to the polycondensation reaction.

The critical aspect here is that increasing alkalinity provides more hydroxyl ions (OH–) in the reaction medium. These ions catalyze the hydrolysis of ester linkages, effectively increasing the concentration of reactive species that can participate in crosslinking. This results in a higher crosslinking density in the resulting polymer. The enhanced crosslink density, in turn, contributes significantly to the exceptional rejection properties observed, primarily based on size exclusion.

The stability and durability of nanofiltration composite membranes are crucial for filtration applications [42]. In our research, where we introduced two distinct monomers into the aqueous phase, it is essential to conduct an extended-term assessment to ensure the long-lasting performance of the TFC membranes. As a result, we examined the permeation properties of the TFC membranes for three days, utilizing a 1.0 gL^{-1} NaCl feed at 70 psi, as depicted in Fig. 6. The results demonstrate the impressive durability of the TFC membrane, with consistent permeate flux and rejection characteristics throughout the testing period, at approximately 59 $Lm^{-2}h^{-1}$ and 35 %, respectively.

Table 3 compares the performance of our membranes with that of the most recently published works on fabricating polyester and polyesteramide membranes for NF applications. One notable advancement involved using hyperbranched polyester (HPE) in an interfacial polymerization process [17]. This method effectively reduced the diffusion rate of PIP by capitalizing on HPE's steric hindrance and its ability to engage in hydrogen bonding interactions, resulting in remarkable pure water permeability (50.62 $Lm^{-2}h^{-1}bar^{-1}$) coupled with over 98 % Na_2SO_4 rejection. This membrane also exhibited long-term stability and outstanding antifouling properties.

In another research, sugar-based nanofiltration membranes were created using glucose, maltose, and raffinose as monomers through interfacial polymerization [10]. These membranes exhibited a remarkable water permeance of 30–34 $Lm^{-2}h^{-1}bar^{-1}$ at the expense of a slight reduction in Na_2SO_4 rejection to 95 %. The high permeability of these membranes was attributed to the highly hydrophilic and thin polyester layer. Lü et al. introduced a TFC nanofiltration membrane with an asymmetric separation layer that showed promise for wastewater treatment in dye and textile industries [43]. Their composite membrane consisted of a loose poly(piperazine amide) (PA) layer and a tannic acid (TA) skin. When compared to a membrane with a symmetric PA layer, their composite membrane exhibited a 28.0 % higher pure water permeability, significantly increased water fluxes for anionic dyes (alizarin yellow R, sunset yellow, Congo red) by 50.3 %, 43.9 %, and 36.1 %, and a noteworthy reduction in steady-state flux declines by 27.8 %, 43.4 %, and 23.5 %. Furthermore, the PA/TA-based membrane displayed enhanced antifouling properties and alizarin yellow R rejection. Another notable innovation in this domain involved the synthesis of antifouling polyester-amide loose nanofiltration membranes by interfacial polymerization for zero liquid discharge in dye/salt wastewater treatment [22]. The membrane provided exceptional water permeability

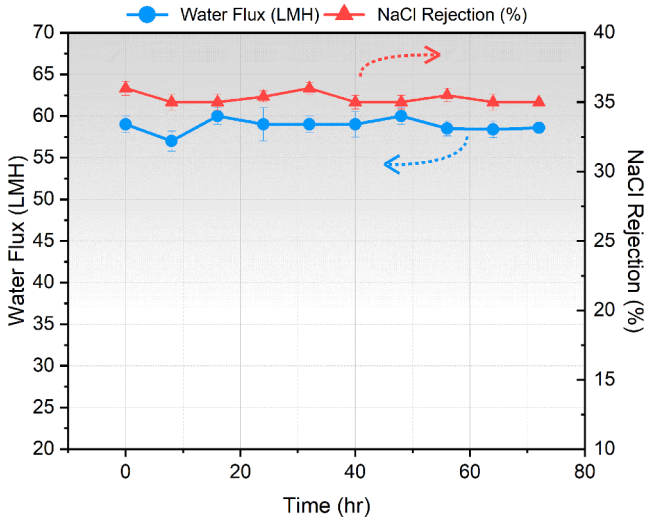

Fig. 6. Long-time stability test of TFC membrane (PEA-10 %-12). Testing conditions: 70 psi, 25 ± 3 °C.

Table 3
Membrane performance of some recent PE and PEA membranes, including the fabricated membranes in current research.

Aq. Phase Monomer	Org. phase monomer	Water permeance (LMH.bar-1)	Salt ejection (%)	Dye rejection (%)	Key Feature(s)	Reference
Glucose	TMC	34.2	Na_2SO_4: 65NaCl: 12	MO: 92	High antifouling performance and a good option for dye/salt separation	PE-12 (This Work)
PIP + Glucose	TMC	12	Na_2SO_4: 99.5NaCl: 59	MO: 99.5	High Fouling resistance and stability, and a favorable choice for the separation of divalent salts	PEA-10 %-12 (This Work)
PIP + HPE	TMC	50	Na_2SO_4: ~99	–	Highly permeable and stable polyester-amide membrane with 99 % Na_2SO_4 rejection	[17]
Glucose, Maltose, Raffinose	TMC	30–34	Na_2SO_4 94–95	–	High water permeability and up to 95 % Na_2SO_4 rejection	[10]
PIP/Tannic acid	TMC	10.3	Na_2SO_4: 99.4NaCl: 71.2	Alizarin yellow R 97.5 Sunset yellow 99.9 Congo red 99.9	Superior pure water permeability, improved anionic dye removal, and enhanced antifouling performance	[43]
Bis-tris propane	TMC	23	Na_2SO_4: <30NaCl: 11.72	ReactiveBlack 5: 98.8	High separation of dye/salt mixtures and antifouling and stability performance.	[22]
Glucose	TMC	16.1	Na_2SO_4: 99.5 NaCl: 53.2	_	High flux, salt rejection, chlorine resistance, and stability compared to conventional PA membranes	[21]

(114.9 $Lm^{-2}h^{-1}$) and excellent dye rejection (98.83 % RB 5). In yet another study, a thermal-facilitated interfacial polymerization approach was employed to create high-performance polyester TFC membranes [21]. Elevated temperatures expedited monomer diffusion and reaction rates, developing a PE layer with 99.5 % Na_2SO_4 rejection and 16.1 $Lm^{-2}h^{-1}bar^{-1}$ water permeance. Also, these membranes demonstrated remarkable chlorine resistance (960,000 ppm h) and maintained their separation efficiency even after exposure to a sodium hypochlorite solution (1000 ppm) for 36 days. It is worth noting that this research represents a pioneering effort in investigating the impact of monomer ratio and alkalinity of the aqueous solution on the chemical and morphological properties of the TFC membranes. As illustrated in Fig. 5, the NF membranes can be tailored for entirely distinct applications by modifying the monomer ratio and adjusting the pH of the aqueous

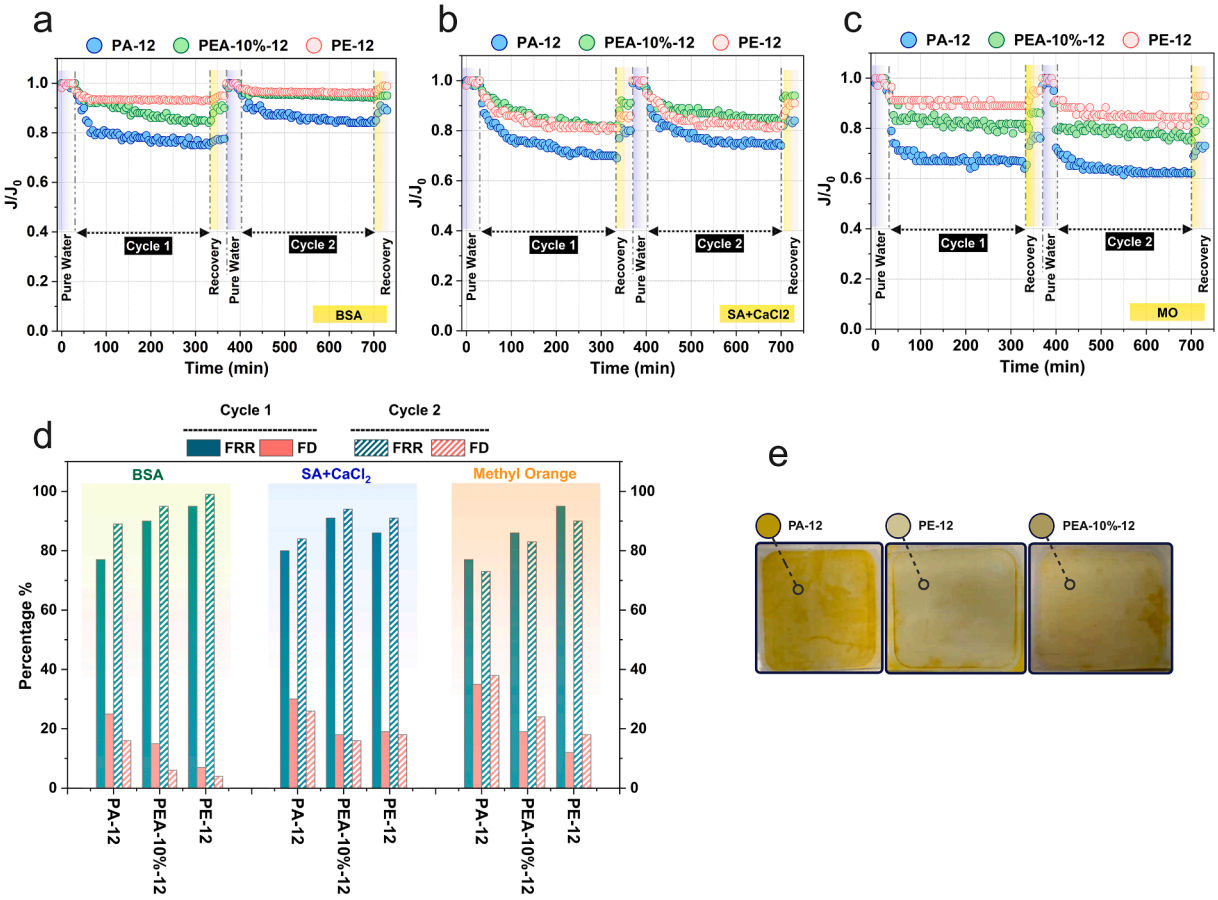

Fig. 7. Normalized water flux versus filtration time of PA-12, PEA-10 %-12, and PE-12 during the (a) BSA, (b) SA + $CaCl_2$, and (c) methyl orange solution filtration in two 6-h cycles. (d) Flux decline (FD) and flux recovery ratio (FRR) of PA-L, PA-X, and PE-7 for all fouling experiments. The concentration of BSA was 100 ppm, and the concentration of SA and methyl orange was 150 ppm. (e) Pictures of PA-12, PE-12, and PEA-10 %-12 coupons after fouling experiments with methyl orange. (For interpretation of the references to colour in this figure legend, the reader is referred to the web version of this article.)

solution.

3.5. Antifouling properties of TFC membranes

The data presented in Fig. 7 depicts the normalized water flux over time, the flux recovery ratio, and the flux decline for three different membranes: PE-12, PEA-10 %-12, and PA-12. When comparing these membranes, it's evident that the polyester membrane (PE-12) notably exhibits a smaller decline in flux during a 5-hour filtration period when subjected to fouling solutions containing BSA and MO. This underscores the vital role of glucose monomers in enhancing the membrane's antifouling properties. In the case of BSA fouling, PE-12 stands out with the highest flux recovery ratio at 95.5 %, followed by PEA-10 %-12 at 91 % and PA-12 at 78.5 %. When MO is the fouling agent, PE-12 again outperforms with a flux recovery ratio of 95 %, compared to 86 % for PEA-10 % and 77 % for PA-12. This difference can be attributed to the smaller size of methyl orange, which may facilitate its penetration into membrane pores, leading to fouling. Fig. 7(e) provides a visual comparison of membrane coupons after undergoing two filtration cycles with methyl orange. When MO is the fouling agent, PE-12 again outperforms with a flux recovery ratio of 95 %, compared to 86 % for PEA-10 % and 77 % for PA-12. This difference can be attributed to the smaller size of methyl orange, which may facilitate its penetration into membrane pores, leading to fouling. The superior antifouling properties of polyester and polyesteramide membranes can be attributed to three key factors: changes in membrane hydrophilicity, surface charge, and surface roughness, primarily influenced by the presence of glucose monomers [44]. The incorporation of glucose enhances the hydrophilicity of the membranes, thereby preventing foulants from adhering to the membrane surface due to the formation of a hydration layer [45]. Furthermore, glucose-based TFC membranes are more negatively charged, mitigating the attachment of predominantly negatively charged foulants due to electrostatic repulsion. Lastly, glucose monomers lead to the formation of a smoother surface with fewer attachment points for foulants. This, in turn, simplifies the cleaning process, as deep irregularities that could harbor fouling materials are reduced. Reduced surface roughness also improves the hydrodynamic conditions on the membrane surface, allowing for more efficient foulant removal and, as a result, reduced fouling accumulation [46]. Nevertheless, when exposed to a fouling solution containing SA + $CaCl_2$, the polyester membrane (PE-12) exhibits slightly lower FRR and FD values compared to PEA-12–10 %. This decline can be attributed to the higher concentration of free carboxylic groups in the structure of polyester membranes, intensifying calcium bridging between the membrane surface and foulants, thus exacerbating fouling [47].

3.6. Discussion

This study has underscored the critical role of monomers in determining the structure and morphology of TFC membranes. The empirical evidence presented in our study demonstrates that the rate and intensity of the polymerization reaction between the aqueous solution monomer (PIP and glucose) and organic solution monomer (TMC), as well as the size and mass transfer properties of the monomers, substantially influence the final structure of the membrane. The reaction rate of PIP and TMC in the formation of polyamide is typically faster than the reaction rate of glucose and TMC. This is due to the different molecular structures and reactivity of the compounds involved, as well as different bond formations and functional groups. When PIP and TMC react, a polycondensation reaction occurs, resulting in the formation of a polyamide. In this reaction, the amine group of PIP (NH_2) reacts with the acid chloride functional groups (−COCl) of TMC to form amide bonds (−CONH–) and release HCl. This condensation reaction occurs relatively quickly because PIP is a primary amine with high reactivity to the acid chloride groups of TMC. Furthermore, because both molecules have multiple reactive sites, the formation of amide bonds is facilitated. Glucose, on the other hand, is a larger molecule with multiple hydroxyl groups (−OH) that reacts with TMC to form a glucose-based TFC in a similar polycondensation reaction. In comparison to PIP and TMC, however, the reaction rate of glucose with TMC is generally slower. This is primarily due to the higher molecular weight of glucose, which can slow down their reactivity to the TMC.

Based on the preceding discussion, the selective layer formation in PA membranes occurs via a faster interfacial polymerization process with TMC than in PEA and PE membranes, respectively. The reaction rate influences the extent to which polymer chains are formed at a constant time [48]. A faster reaction rate enables more efficient polymerization, which results in longer polymer chains and a higher degree of polymerization [32]. As a result, the thin film layer formed may be denser and more selective. Additionally, the reaction rate influences the molecular weight of the polymer, with faster reaction rates generally leading to the production of polymers with higher molecular weights [49]. A slower reaction rate allows the polymer chains more time to arrange and organize, resulting in a more ordered and smooth membrane surface, as seen in AFM results of the membranes. Furthermore, a slower reaction rate allows for better reactant mixing and diffusion, resulting in a more homogeneous TFC layer (in agreement with SEM and AFM data) [50].

The change in reaction pH was one of the main parameters considered for this study. The reaction rate between monomers and TMC increases as the pH value rises. In an alkaline environment, the nucleophilic amine group in PIP and the hydroxyl group in glucose become more reactive, increasing their interaction with the acid chloride groups in TMC. At higher pH, nucleophilic groups are more likely to be deprotonated. For instance, the amine group forms free amine (RNH_2), a stronger nucleophile due to the availability of the lone pair of electrons, increasing the reactivity and the reaction kinetic in basic conditions. The acceleration in reaction rate has the potential to enhance polymerization efficiency, leading to the formation of longer polymer chains and an increased degree of polymerization. This, in turn, yields a membrane characterized by enhanced structural stability and mechanical robustness, which justifies the higher rejection rates and lower water flux of the membranes synthesized under more alkaline conditions.

4. Conclusion

This study has demonstrated the significant influence of monomer choice and reaction pH on the structural and functional characteristics of TFC membranes. The glucose-based membranes displayed improved hydrophilicity and a negative surface charge, enhancing their antifouling properties. Adjusting pH during fabrication had distinct effects, with higher pH values leading to a higher crosslinked TFC layer, which increased rejection rates but reduced water flux, while lower pH values had the opposite effect. Moreover, pH variation during membrane fabrication influenced surface charge and hydrophilicity. In terms of performance, PA membranes outperformed others, achieving notable rejection rates. In contrast, PE membranes exhibited the highest water flux. Notably, TFC membranes with a specific monomer combination achieved a balanced performance profile, while some exhibited exceptional antifouling properties. These findings underscore the practical significance of tailoring membrane properties for high-performance water treatment applications by adjusting pH and monomer selection. This study provides a solid foundation for developing more effective TFC membranes. In the context of scaling up, it becomes increasingly critical to confront the challenges associated with high pH conditions. Elevated pH environments pose safety risks and processing challenges, including fouling and corrosion, which can profoundly affect the effectiveness and durability of large-scale TFC membrane production. Hence, conducting a meticulous risk assessment and choosing materials capable of withstanding highly alkaline conditions are paramount to guarantee the success of upscaling TFC membrane fabrication under such alkaline

conditions.

Future research in this area holds tremendous promise. It could involve the exploration of more complex chemistries in the TFC layer by incorporating a wider range of monomers and adjusting the contribution of each monomer through variations in reaction conditions, such as pH and temperature. This fine-tuning offers exciting prospects for engineering the TFC layer's structure, enabling the creation of membranes tailored for specific applications. By embracing this approach, researchers can strive to optimize key factors such as rejection rates, water flux, and antifouling properties, aligning the properties of TFC membranes more precisely with the requirements of diverse industries and water treatment scenarios. The pursuit of enhanced customization and performance could lead to more efficient and sustainable solutions for global water purification and resource management challenges.

Declaration of competing interest

The authors declare that they have no known competing financial interests or personal relationships that could have appeared to influence the work reported in this paper.

Data availability

No data was used for the research described in the article.

Acknowledgment

Financial support for this work through Canada's Oil Sand Innovation Alliance (COSIA) and the Natural Sciences and Engineering Research Council of Canada (NSERC) is gratefully acknowledged.

References

[1] J. Liu, H. Yang, S.N. Gosling, M. Kummu, M. Flörke, S. Pfister, N. Hanasaki, Y. Wada, X. Zhang, C. Zheng, J. Alcamo, T. Oki, Water scarcity assessments in the past, present, and future, Earth's Future (2017), https://doi.org/10.1002/2016EF000518.

[2] Unesco, The united nations world water development report 2021: valuing water, Water Politics, 2021.

[3] Cevallos-Mendoza, J.; Amorim, C. G.; Rodríguez-Díaz, J. M.; Montenegro, M. da C. B. S. M. Removal of Contaminants from Water by Membrane Filtration: A Review. *Membranes*. 2022. https://doi.org/10.3390/membranes12060570.

[4] T. Lu, W. Cao, H. Liang, Y. Deng, Y. Zhang, M. Zhu, W. Ma, R. Xiong, C. Huang, Blow-spun nanofibrous membrane for simultaneous treatment of emulsified oil/water mixtures, dyes, and bacteria, Langmuir 38 (50) (2022), https://doi.org/10.1021/acs.langmuir.2c02620.

[5] M.Q. Seah, W.J. Lau, P.S. Goh, H.H. Tseng, R.A. Wahab, A.F. Ismail, Progress of interfacial polymerization techniques for polyamide thin film (nano)composite membrane fabrication: a comprehensive review, Polymers (2020), https://doi.org/10.3390/polym12122817.

[6] Asad, A.; Aghapour Aktij, S.; Karami, P.; Sameoto, D.; Sadrzadeh, M. Micropatterned Thin-Film Composite Poly(Piperazine-Amide) Nanofiltration Membranes for Wastewater Treatment. *ACS Appl Polym Mater 3* (12), 6653–6665. https://doi.org/10.1021/acsapm.1c01096.

[7] W.J. Lau, S. Gray, T. Matsuura, D. Emadzadeh, J. Paul Chen, A.F. Ismail, A review on polyamide thin film nanocomposite (tfn) membranes: history, applications Challenges and Approaches, *Water Research.* (2015), https://doi.org/10.1016/j.watres.2015.04.037.

[8] S.A. Aktij, M. Hosseininejad, M. Dadashi Firouzjaei, S. Farhadi, M. Elliott, A. Rahimpour, J.B.P. Soares, M. Sadrzadeh, Y. Mansourpanah, High permselectivity and performance of tuned nanofiltration membranes by merging carbon nitride derivatives as interphase layer for efficient water treatment, J. Water Process Eng. 56 (2023), 104432, https://doi.org/10.1016/j.jwpe.2023.104432.

[9] B. Khorshidi, T. Thundat, B.A. Fleck, M. Sadrzadeh, Thin film composite polyamide membranes: parametric study on the influence of synthesis conditions, RSC Adv. 5 (68) (2015) 54985–54997, https://doi.org/10.1039/C5RA08317F.

[10] J. Zheng, Y. Liu, J. Zhu, P. Jin, T. Croes, A. Volodine, S. Yuan, B. Van der Bruggen, Sugar-based membranes for nanofiltration, J Memb Sci 619 (2021), https://doi.org/10.1016/j.memsci.2020.118786.

[11] Z. Zhang, K. Fan, Y. Liu, S. Xia, A review on polyester and polyester-amide thin film composite nanofiltration membranes: synthesis, characteristics and applications, Sci. Total Environ. (2023), https://doi.org/10.1016/j.scitotenv.2022.159922.

[12] Q. Fan, T. Lu, Y. Deng, Y. Zhang, W. Ma, R. Xiong, C. Huang, Bio-based materials with special wettability for oil-water separation, Sep. Purif. Technol. (2022), https://doi.org/10.1016/j.seppur.2022.121445.

[13] H. Zhang, F. Xie, Z. Zhao, N.U. Afsar, F. Sheng, L. Ge, X. Li, X. Zhang, T. Xu, Novel poly(ester amide) membranes with tunable crosslinked structures for nanofiltration, ACS Appl Mater Interfaces 14 (8) (2022), https://doi.org/10.1021/acsami.1c21862.

[14] H. Guo, L.E. Peng, Z. Yao, Z. Yang, X. Ma, C.Y. Tang, Non-polyamide based nanofiltration membranes using green metal-organic coordination complexes: implications for the removal of trace organic contaminants, Environ Sci Technol 53 (5) (2019), https://doi.org/10.1021/acs.est.8b06422.

[15] N.A. Ahmad, P.S. Goh, Z.A. Karim, A.F. Ismail, Thin film composite membrane for oily waste water treatment: recent advances and challenges, Membranes (Basel) 8 (2018), https://doi.org/10.3390/membranes8040086.

[16] A. Shakeri, H. Salehi, F. Ghorbani, M. Amini, H. Naslhajian, Polyoxometalate based thin film nanocomposite forward osmosis membrane: superhydrophilic, antifouling, and high water permeable, J Colloid Interface Sci 536 (2019), https://doi.org/10.1016/j.jcis.2018.10.069.

[17] J. Tian, B. Song, S. Gao, B. Van der Bruggen, R. Zhang, Omnifarious performance promotion of the tfc nf membrane prepared with hyperbranched polyester intervened interfacial polymerization, J Memb Sci 642 (2022), https://doi.org/10.1016/j.memsci.2021.119984.

[18] F.L. Aachmann, D.E. Otzen, K.L. Larsen, R. Wimmer, Structural background of cyclodextrin-protein interactions, Protein Eng 16 (12) (2003), https://doi.org/10.1093/protein/gzg137.

[19] J. Xue, Z. Jiao, R. Bi, R. Zhang, X. You, F. Wang, L. Zhou, Y. Su, Z. Jiang, Chlorine-resistant polyester thin film composite nanofiltration membranes prepared with β-cyclodextrin, J Memb Sci 584 (2019), https://doi.org/10.1016/j.memsci.2019.04.077.

[20] J. Zhao, Y. Su, X. He, X. Zhao, Y. Li, R. Zhang, Z. Jiang, Dopamine composite nanofiltration membranes prepared by self-polymerization and interfacial polymerization, J Memb Sci 465 (2014), https://doi.org/10.1016/j.memsci.2014.04.018.

[21] J. Shen, G. Wang, X. You, B. Shi, J. Xue, J. Yuan, Y. Li, J. Guan, Y. Ma, Y. Su, R. Zhang, Z. Jiang, Thermal-facilitated interfacial polymerization toward high-performance polyester desalination membrane, J Mater Chem A Mater 9 (13) (2021), https://doi.org/10.1039/d0ta12283a.

[22] J. Cheng, Z. Li, X. Bao, R. Zhang, S. Yin, W. Huang, K. Sun, W. Shi, A novel polyester-amide loose composite nanofiltration membrane for effective dye/salt separation: the effect of long molecule on the interfacial polymerization, J Memb Sci 657 (2022), 120675, https://doi.org/10.1016/J.MEMSCI.2022.120675.

[23] Q. Hu, D. Li, S. Liu, G. Yan, J. Yang, G. Zhang, Effects of alkali on the polyester membranes based on cyclic polyphenols for nanofiltration, Desalination 533 (2022), 115774, https://doi.org/10.1016/J.DESAL.2022.115774.

[24] C. Lai, X. Zhu, J. Li, W. Zhou, J. Xu, J. Ding, J. Song, D. Wu, H. Liang, X. Cheng, PH-regulated interfacially polymerized nanofiltration membranes to achieve high separation of nom and moderate desalination for purifying ground water, Desalination 544 (2022), 116148, https://doi.org/10.1016/J.DESAL.2022.116148.

[25] N. Helali, L. Shamaei, M. Rastgar, M. Sadrzadeh, Development of layer-by-layer assembled polyamide-imide membranes for oil sands produced water treatment, Sci Rep 11 (1) (2021), https://doi.org/10.1038/s41598-021-87601-4.

[26] L. Shamaei, B. Khorshidi, M.A. Islam, M. Sadrzadeh, Industrial waste lignin as an antifouling coating for the treatment of oily wastewater: creating wealth from waste, J Clean Prod 256 (2020), https://doi.org/10.1016/j.jclepro.2020.120304.

[27] L. Shamaei, P. Karami, B. Khorshidi, R. Farnood, M. Sadrzadeh, Novel lignin-modified forward osmosis membranes: waste materials for wastewater treatment, ACS Sustain Chem Eng 9 (47) (2021), https://doi.org/10.1021/acssuschemeng.1c03861.

[28] M.Q. Seah, W.J. Lau, P.S. Goh, B.S. Ooi, G.S. Lai, A.F. Ismail, Improving properties of thin film nanocomposite membrane via temperature-controlled interfacial polymerization for nanofiltration process, Desalination 545 (2023), https://doi.org/10.1016/j.desal.2022.116091.

[29] F. Gao, H. Liu, Y. Zhang, D. Liu, Z. Xie, W. Peng, Y. Song, R. Hu, D. Chen, J. Kang, R. Xu, Y. Cao, M. Xiang, Polyamide membrane with nanoscale stripes and internal voids for high-performance nanofiltration, SSRN Electron. J. (2022), https://doi.org/10.2139/ssrn.4297298.

[30] P. Karami, M.M.H. Mizan, C. Ammann, A. Taghipour, J.B.P. Soares, M. Sadrzadeh, Novel lignosulfonated polyester membranes with remarkable permeability and antifouling characteristics, J Memb Sci 687 (2023), 122034, https://doi.org/10.1016/J.MEMSCI.2023.122034.

[31] P. Karami, B. Khorshidi, J.B.P. Soares, M. Sadrzadeh, Fabrication of highly permeable and thermally stable reverse osmosis thin film composite polyamide membranes, ACS Appl Mater Interfaces 12 (2) (2020), https://doi.org/10.1021/acsami.9b16875.

[32] B. Khorshidi, T. Thundat, B.A. Fleck, M. Sadrzadeh, Thin film composite polyamide membranes: parametric study on the influence of synthesis conditions, RSC Adv 5 (68) (2015), https://doi.org/10.1039/c5ra08317f.

[33] B. Khorshidi, T. Thundat, B.A. Fleck, M. Sadrzadeh, A novel approach toward fabrication of high performance thin film composite polyamide membranes, Sci Rep (2016) 6, https://doi.org/10.1038/srep22069.

[34] Y. Yao, P. Zhang, C. Jiang, R.M. DuChanois, X. Zhang, M. Elimelech, High performance polyester reverse osmosis desalination membrane with chlorine resistance, Nat Sustain 4 (2) (2021), https://doi.org/10.1038/s41893-020-00619-w.

[35] Chandra, P. N.; Usha, K.; Mohan, M. K. Design, Development and Characterization of Polyelectrolyte Multilayer Membranes for Potential Filtration Applications. In *Materials Today: Proceedings*; 2020; Vol. 41. https://doi.org/10.1016/j.matpr.2020.05.239.

[36] M. Dalwani, N.E. Benes, G. Bargeman, D. Stamatialis, M. Wessling, Effect of PH on the performance of polyamide/polyacrylonitrile based thin film composite membranes, J Memb Sci 372 (1–2) (2011), https://doi.org/10.1016/j.memsci.2011.02.012.
[37] G.R. Xu, J.N. Wang, C.J. Li, Strategies for improving the performance of the polyamide thin film composite (pa-tfc) reverse osmosis (ro) membranes: surface modifications and nanoparticles incorporations, Desalination (2013), https://doi.org/10.1016/j.desal.2013.08.022.
[38] Y.S. Khoo, W.J. Lau, Y.Y. Liang, M. Karaman, M. Gürsoy, A.F. Ismail, A green approach to modify surface properties of polyamide thin film composite membrane for improved antifouling resistance, Sep Purif Technol (2020) 250, https://doi.org/10.1016/j.seppur.2020.116976.
[39] H.M. Hegab, Y. Wimalasiri, M. Ginic-Markovic, L. Zou, Improving the fouling resistance of brackish water membranes via surface modification with graphene oxide functionalized chitosan, Desalination (2015) 365, https://doi.org/10.1016/j.desal.2015.02.029.
[40] M.F. Ismail, M.A. Islam, B. Khorshidi, A. Tehrani-Bagha, M. Sadrzadeh, Surface characterization of thin-film composite membranes using contact angle technique: review of quantification strategies and applications, Adv Colloid Interface Sci 299 (2022), 102524.
[41] R.N. Wenzel, Surface roughness and contact angle, J. Phys. Colloid Chem. 53 (9) (1949) 1466–1467, https://doi.org/10.1021/j150474a015.
[42] Z. Lv, J. Hu, X. Zhang, L. Wang, Enhanced surface hydrophilicity of thin-film composite membranes for nanofiltration: an experimental and dft study, PCCP (2015) 17 (37), https://doi.org/10.1039/c5cp04105h.
[43] Z. Lü, F. Hu, H. Li, X. Zhang, S. Yu, M. Liu, C. Gao, Composite nanofiltration membrane with asymmetric selective separation layer for enhanced separation efficiency to anionic dye aqueous solution, J Hazard Mater (2019) 368, https://doi.org/10.1016/j.jhazmat.2019.01.086.
[44] M. Hayatbakhsh, M. Sadrzadeh, D. Pernitsky, S. Bhattacharjee, J. Hajinasiri, Treatment of an in situ oil sands produced water by polymeric membranes. desalination Water Treat (2016) 57 (32), https://doi.org/10.1080/19443994.2015.1069216.
[45] Z. Xiong, J. Liu, Y. Yang, Q. Lai, X. Wu, J. Yang, Q. Zeng, G. Zhang, S. Zhao, Reinforcing hydration layer on membrane surface via nano-capturing and hydrothermal crosslinking for fouling reduction, J Memb Sci (2022) 644, https://doi.org/10.1016/j.memsci.2021.120076.
[46] G. dong Kang, Y. Ming Cao, Development of antifouling reverse osmosis membranes for water treatment: A review, Water Res. (2012), https://doi.org/10.1016/j.watres.2011.11.041.
[47] Y. Mo, A. Tiraferri, N.Y. Yip, A. Adout, X. Huang, M. Elimelech, Improved antifouling properties of polyamide nanofiltration membranes by reducing the density of surface carboxyl groups, Environ Sci Technol (2012) 46 (24), https://doi.org/10.1021/es303673p.
[48] Z. Wang, S. Liang, Y. Kang, W. Zhao, Y. Xia, J. Yang, H. Wang, X. Zhang, Manipulating interfacial polymerization for polymeric nanofilms of composite separation membranes, Prog. Polym. Sci. (2021), https://doi.org/10.1016/j.progpolymsci.2021.101450.
[49] L. Infante Teixeira, K. Landfester, H. Thérien-Aubin, Nanoconfinement in miniemulsion increases reaction rates of thiol-ene photopolymerization and yields high molecular weight polymers, Polym Chem (2022), https://doi.org/10.1039/d2py00350c.
[50] Y. Jin, Z. Su, Effects of polymerization conditions on hydrophilic groups in aromatic polyamide thin films, J Memb Sci 330 (1–2) (2009), https://doi.org/10.1016/j.memsci.2008.12.055.